Taper-based scattering formulation of the Helmholtz equation to improve the training process of Physics-Informed Neural Networks

W. Dörfler[a], M. Elasmi[a,*], T. Laufer[a,*]

[a]*Karlsruhe Institute of Technology (KIT), Institute for Applied and Numerical Mathematics (IANM), Englerstr. 2, 76131 Karlsruhe, Germany*

Abstract

This work addresses the scattering problem of an incident wave at a junction connecting two semi-infinite waveguides, which we intend to solve using Physics-Informed Neural Networks (PINNs). As with other deep learning-based approaches, PINNs are known to suffer from a spectral bias and from the hyperbolic nature of the Helmholtz equation. This makes the training process challenging, especially for higher wave numbers. We show an example where these limitations are present. In order to improve the learning capability of our model, we suggest an equivalent formulation of the Helmholtz Boundary Value Problem (BVP) that is based on splitting the total wave into a tapered continuation of the incoming wave and a remaining scattered wave. This allows the introduction of an inhomogeneity in the BVP, leveraging the information transmitted during back-propagation, thus, enhancing and accelerating the training process of our PINN model. The presented numerical illustrations are in accordance with the expected behavior, paving the way to a possible alternative approach to predicting scattering problems using PINNs.

Keywords: scattering problems, Helmholtz equation, Dirichlet-to-Neumann operator, PINNs, spectral bias, training process

1. Introduction

Since their introduction in 2019 by Raissi et al. [1], Physics-Informed Neural Networks (PINNs) have gained a huge popularity and interest in the scientific machine learning community and beyond. Remarkable results have been achieved across a wide range of engineering and physical problems. This involves studying both forward problems, e.g., [2–4] and inverse problems, such as [5–7]. For a comprehensive review and discussion on PINNs, refer to [8]. Despite being undeniably promising, PINNs still face several challenges, particularly for forward problems that exhibit higher frequencies, sharp transitions, and complex computational domains [9–11]. Nevertheless, PINNs framework's flexibility has enabled the development of several extensions of the vanilla version that target various PINN-related issues. One such extension is the Self-Adaptive Physics-Informed Neural Network (SA-PINN) [12], which allows to adaptively correct possible discrepancies in the convergence rates for multiple-terms loss functions. Similarly, [10] studied and analyzed the latter problem using the Neural Tangent Kernel (NTK), proposing a deterministic approach to compute suitable scalar weightings of the different loss function's components. In the same context of NTK-theory, [11] introduced Fourier-feature networks to counteract the spectral bias of PINNs. On another note, domain decomposition approaches such as Extended Physics-Informed Neural Networks (XPINNs) [13] provide a high potential framework to deal with large and complex computational domains. In this work, we address the scattering problem of an incident wave at a junction connecting two semi-infinite closed waveguides. Such problems have been studied and analyzed using classical numerical techniques, both theoretically and numerically using the Finite Element Method (FEM), for instance. An application can involve scattered elastic waves, however, we consider the simpler case of an optical wave. The underlying problem is governed by the Helmholtz equation, and a set of mixed boundary conditions using the Dirichlet-to-Neumann (DtN) operator. We refer, e.g., to [14–16], for more details. Solving the Helmholtz equation is challenging due to its hyperbolic nature and structure, even with classical iterative methods [17, 18], particularly for higher wave numbers. This challenge persists and is more pronounced when the solution framework is deep learning-based. To mitigate this, considering adaptive sine activation functions, hyper-parameter tuning, or extending the commonly considered fully-connected neural network by Fourier-feature mappings, enhances significantly the training capabilities of PINNs, see [19–21], respectively. Furthermore, we refer to [22] for a study on the challenges and feasibility of solving the Helmholtz equation in 3D. Perceiving the training difficulty of the considered Helmholtz Boundary Value Problem (BVP) with PINNs, in particular when no sources are present, we propose an equivalent taper-based scattering formulation that introduces inhomogeneities to the right-hand side of the Helmholtz equation and on the homogeneous Dirichlet boundary parts. We begin this article by introducing the classical formulation and the proposed taper-based scattering formulation of the Helmholtz BVP. Next, we briefly define the considered PINN model. In the penultimate section, we present the training results for both formulations using the same PINN

model for different wave numbers, and discuss our findings. Finally, we conclude the work with a brief summary and an outlook for possible improvements in future research.

2. The scattering problem

In this section, we introduce the considered scattering problem of an incident wave at a two-dimensional waveguide junction. As illustrated in Figure 1, the geometric setting consists of the junction $\Omega \subset (-b, b) \times \mathbb{R}$, $b > 0$, connecting two straight semi-infinite closed waveguides, designated by Ω_- and Ω_+. The waveguide junction is assumed to be bounded with boundary $\partial\Omega := \Gamma_- \cup \Gamma_{0,1} \cup \Gamma_{0,2} \cup \Gamma_+$. Thereby, $\Gamma_- := \bar{\Omega}_- \cap \bar{\Omega}$ and $\Gamma_+ := \bar{\Omega}_+ \cap \bar{\Omega}$ denote the interfaces between the waveguides and the junction, and constitute the fixed parts of the junction's shape, whereas $\Gamma_0 := \Gamma_{0,1} \cup \Gamma_{0,2}$ corresponds to the freely designable part. Note that the main geometric requirement that needs to be accounted for is guaranteeing a sufficiently regular boundary across the interfaces, e.g., with a C^2-smooth boundary. We refer to [16] for more details and a thorough formulation of the considered framework. Given an appropriate incoming wave u^{inc} from Ω_- and propagating towards Ω, we consider in this work the case of a closed waveguide junction that satisfies the Helmholtz Boundary Value Problem (BVP), as defined in [16]. First, the notion of a Dirichlet-to-Neumann (DtN) operator is required, see [14] for instance.
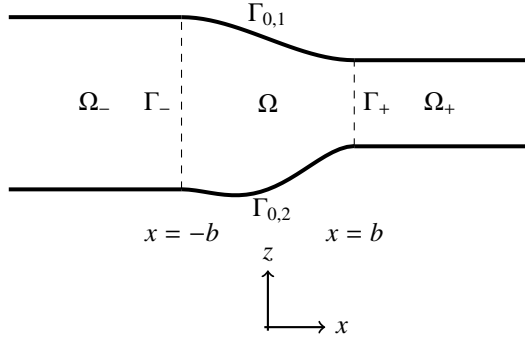

Figure 1: Illustration of the considered type of waveguide junctions Ω. Thereby, Ω_+ and Ω_- denote two semi-infinite waveguides connected by Ω at the interfaces Γ_- (at $x = -b$) and Γ_+ (at $x = b$), respectively. $\Gamma_{0,1}$ and $\Gamma_{0,2}$ designate the remaining boundaries of Ω [16].

Definition 2.1 (Dirichlet-to-Neumann (DtN) operator). Let $\mu_n^2 = n^2\pi^2$, $\phi_n(z) = \sqrt{2}\sin(n\pi z)$ for $z \in (0, 1)$, and $k > 0$. Provided $k^2 \neq \mu_n^2$ for all $n \in \mathbb{N}$, the DtN operator is defined for $w \in L^2((0, 1))$ by

$$\Lambda w := w \mapsto \sum_{n\in\mathbb{N}} \iota\lambda_n (\phi_n, w)_{L^2((0,1))} \phi_n.$$

Thereby, $\lambda_n := \begin{cases} \sqrt{k^2 - \mu_n^2}, & k^2 > \mu_n^2 \\ \iota\sqrt{\mu_n^2 - k^2}, & k^2 \leq \mu_n^2 \end{cases}$ denotes the longitudinal frequency and ι the imaginary unit.

Then, the governing equations can be formulated as follows.

Problem 2.1 (Classical Helmholtz BVP). Let Ω be a bounded waveguide junction as defined above with boundary $\Gamma := \Gamma_{0,1} \cup \Gamma_{0,2} \cup \Gamma_+ \cup \Gamma_-$, and let ν denote a corresponding outer-pointing normal vector. For a wave number $k > 0$, find $u \in C^2(\Omega) \cap C^1(\bar{\Omega})$, $(x, z) \mapsto u(x, z)$ such that

$$\begin{aligned} \Delta u + k^2 u &= 0 & &\text{in } \Omega, \\ u &= 0 & &\text{on } \Gamma_{0,1} \cup \Gamma_{0,2}, \\ \partial_\nu u &= \Lambda u - 2\Lambda u^{\text{inc}} & &\text{on } \Gamma_-, \\ \partial_\nu u &= \Lambda u & &\text{on } \Gamma_+. \end{aligned}$$

Thereby, $\partial_\nu u$ denotes the standard Neumann trace of u, and Λ the DtN operator.

In addition, we propose the consideration of an equivalent formulation of Problem 2.1, which we call the taper-based scattering formulation of the Helmholtz equation. The main idea of the ansatz consists in splitting the unknown wave function $u = u^{\text{sct}} + \chi u^{\text{inc}}$ to separate the incoming wave u^{inc} and rewrite the problem in terms of the scattered wave u^{sct}. Thereby, we call the function $\chi : (-b, b) \to [0, 1]$ a taper-function and define it as

$$\chi(x) = \begin{cases} \frac{-6}{b^5}x^5 - \frac{15}{b^4}x^4 - \frac{10}{b^3}x^3, & x < 0, \\ 0, & x \geq 0. \end{cases} \tag{1}$$

Per construction, the taper-function satisfies $\chi(-b) = 1$ and $\chi(0) = 0$, and possesses vanishing first and second derivatives at $x = -b$ and $x = 0$ as well. Hence, $\chi \in C^2((-b, b))$. With this and by taking into account that a suitable incoming wave u^{inc} solves Problem 2.1, the equivalent taper-based Helmholtz BVP reads as follows.

Problem 2.2 (Taper-based scattering BVP). For $k > 0$ and χ as defined in (1), find $u^{\text{sct}} \in C^2(\Omega) \cap C^1(\bar{\Omega})$ such that

$$\begin{aligned} \Delta u^{\text{sct}} + k^2 u^{\text{sct}} &= -2\frac{\partial u^{\text{inc}}}{\partial x}\frac{\partial\chi}{\partial x} - u^{\text{inc}}\frac{\partial^2\chi}{\partial x^2} & &\text{in } \Omega, \\ u^{\text{sct}} &= -u^{\text{inc}}\chi & &\text{on } \Gamma_{0,1} \cup \Gamma_{0,2}, \\ \partial_\nu u^{\text{sct}} &= \Lambda u^{\text{sct}} & &\text{on } \Gamma_- \cup \Gamma_+. \end{aligned}$$

After solving Problem 2.2, the total wave u is merely reconstructed by adding $u^{\text{inc}}\chi$ to the solution u^{sct}. Obviously, Problems 2.1 and 2.2 are equivalent, yet structurally different due to the inhomogeneity introduced to the BVP via the splitting. This is expected to improve the prediction capabilities of our model-based deep learning approach, namely Physics-Informed Neural Networks (PINNs), which we briefly introduce in the next section.

3. Physics-Informed Neural Networks

PINN was first introduced in 2019 by Raissi et al. [1]. It consists in a hybrid approach that supplements a given Artificial Neural Network (ANN) by the underlying mathematical model (or parts of it), rendering a successful prediction physically consistent. In its vanilla version, the main building block of a PINN is a deep ANN, which consists of a plain stack of layers. The

first and last layer are known as input and output layer, respectively, whereas the remaining ones correspond to the hidden layers. For $i = 1, \ldots, M$ and $M > 1$, we denote the realization function of the i-th layer by $l_i : \mathbb{R}^{N_{i-1}} \to \mathbb{R}^{N_i}$, where N_i is the number of neurons of the i-th layer. Formally, the network function NN_θ of an ANN mapping an input $x \in \mathbb{R}^{N_0}$ to an output $u_\theta := \mathrm{NN}_\theta(x) \in \mathbb{R}^{N_{M+1}}$ is defined recursively via

$$
\begin{aligned}
l_0 &:= x, \\
l_i &= \sigma_i \left(W_i l_{i-1} + b_i \right), \quad i = 1, \ldots, M, \\
u_\theta &= W_{M+1} l_M + b_{M+1},
\end{aligned}
$$

where σ_i is a possibly non-linear activation function for the i-th layer, and $W_i \in \mathbb{R}^{N_i \times N_{i-1}}$ and $b_i \in \mathbb{R}^{N_i}$ are known as the weight matrices and bias vectors, respectively. For convenience, let $\theta := (W_1, b_1, \ldots, W_{M+1}, b_{M+1})$ denote the set of all trainable parameters of the neural network. Using automatic differentiation [23], derivatives of the ANN's output function can be computed efficiently. This allows the penalization of non-physical solutions during the optimization process by incorporating the model equations into the loss function. For instance, let $\mathcal{L}$ be a differential operator (e.g., Helmholtz operator) and $\mathcal{B}_j$ some boundary operators, defining with suitable right-hand side f and boundary conditions g_j the following BVP

$$
\begin{aligned}
\mathcal{L}[u](x) &= f(x) & x \in \Omega, \\
\mathcal{B}_j[u](x) &= g_j(x) & x \in \Gamma_j \subset \partial\Omega, \; j = 1, \ldots, 4.
\end{aligned} \tag{2}
$$

The PINN ansatz consists in using $u_\theta := \mathrm{NN}_\theta(x)$ as a surrogate model for the solution u, cf. [1]. In practice, training a PINN model without additional data reduces to minimizing an empirical loss function that evaluates the model equations. Concretely, for the training points $x_{\mathrm{r}} = \{x_{\mathrm{r},i}\}_{i=1}^{N_{\mathrm{r}}} \subset \Omega$ and $x_{\mathrm{b}_j} = \{x_{\mathrm{b}_j,i}\}_{i=1}^{N_{\mathrm{b}_j}} \subset \Gamma_j$, $j = 1, \ldots, 4$, a typical loss function reads

$$
L(\theta, x_{\mathrm{r}}, x_{\mathrm{b}}) := L_{\mathrm{r}}(\theta, x_{\mathrm{r}}) + \sum_{j=1}^{4} L_{\mathrm{b}_j}(\theta, x_{\mathrm{b}_j})
$$

with

$$
\begin{aligned}
L_{\mathrm{r}}(\theta, x_{\mathrm{r}}) &= \frac{1}{N_{\mathrm{r}}} \sum_{i=1}^{N_{\mathrm{r}}} \left(\mathcal{L}[u_\theta](x_{\mathrm{r},i}) - f(x_{\mathrm{r},i}) \right)^2, \\
L_{\mathrm{b}_j}(\theta, x_{\mathrm{b}_j}) &= \frac{1}{N_{\mathrm{b}_j}} \sum_{i=1}^{N_{\mathrm{b}_j}} \left(\mathcal{B}_j[u_\theta](x_{\mathrm{b}_j,i}) - g_j(x_{\mathrm{b}_j,i}) \right)^2.
\end{aligned}
$$

The minimization procedure is usually performed using a gradient-descent type optimizer, e.g., Adaptive moment estimation (Adam) [24]. As per all iterative methods, optimizing the ANN's trainable parameters require initialization. Popular choices include the Glorot [25] or He initialization [26], for instance.

Although promising, the vanilla version of PINN suffers from two main pathologies that limit its use cases. The first one, known as the spectral bias, is inherited from the conventional neural networks commonly used for PINNs. It states that neural networks tend to learn functions along the dominant eigendirections, which correspond to the lowest frequencies. In other words, they struggle to learn functions with higher frequencies. We refer the reader, e.g., to [9, 11] and the references therein for more details. The second pathology addresses a possible imbalance in the convergence rates of the constituent terms of the total loss function, which could result in neglecting certain aspects of the solution, hence to training failure, see [10, 27], for instance. Several extensions of PINN that address and (partially) circumvent these effects have been proposed and successfully deployed. However, to the authors knowledge, there is still no generic PINN approach that allows efficient predictions of forward problems based solely on the mathematical model. In this work, we consider the Self-Adaptive Physics-Informed Neural Network (SA-PINN), introduced in [12]. This approach is based on soft attention mechanisms and allows the reduction of convergence discrepancies of the loss terms by introducing a self-adaptive mask function $m : [0, \infty) \to [0, \infty)$ that associates to each training point a trainable weight. The function m is assumed to be differentiable and strictly increasing, see [12] for possible choices of m and their effect on the training procedure. Provided $\lambda_{\mathrm{r}} = (\lambda_{\mathrm{r},1}, \ldots, \lambda_{\mathrm{r},N_{\mathrm{r}}})$ and $\lambda_{\mathrm{b}} := \left(\lambda_{\mathrm{b}_j} \right)_{j=1}^{4}$ with $\lambda_{\mathrm{b}_j} = \left(\lambda_{\mathrm{b}_j,1}, \ldots, \lambda_{\mathrm{b}_j,N_{\mathrm{b}_j}} \right)$ are non-negative, the extended loss function, reads

$$
L(\theta, x_{\mathrm{r}}, x_{\mathrm{b}}, \lambda_{\mathrm{r}}, \lambda_{\mathrm{b}}) = L_{\mathrm{r}}(\theta, x_{\mathrm{r}}, \lambda_{\mathrm{r}}) + \sum_{j=1}^{4} L_{\mathrm{b}_j}(\theta, x_{\mathrm{b}_j}, \lambda_{\mathrm{b}_j}), \tag{3}
$$

where

$$
\begin{aligned}
L_{\mathrm{r}}(\theta, x_{\mathrm{r}}, \lambda_{\mathrm{r}}) &= \frac{1}{N_{\mathrm{r}}} \sum_{i=1}^{N_{\mathrm{r}}} m(\lambda_{\mathrm{r},i}) \left(\mathcal{L}[\theta](x_{\mathrm{r},i}) - f(x_{\mathrm{r},i}) \right)^2, \\
L_{\mathrm{b}_j}(\theta, x_{\mathrm{b}_j}, \lambda_{\mathrm{b}_j}) &= \frac{1}{N_{\mathrm{b}_j}} \sum_{i=1}^{N_{\mathrm{b}_j}} m(\lambda_{\mathrm{b}_j,i}) \left(\mathcal{B}_j[\theta](x_{\mathrm{b}_j,i}) - g_j(x_{\mathrm{b}_j,i}) \right)^2.
\end{aligned}
$$

With this, the optimization problem turns to a saddle point problem that simultaneously minimizes θ, and penalizes the regions with higher losses by maximizing λ_{r} and λ_{b}, i.e., solving

$$
\min_{\theta} \max_{\lambda_{\mathrm{r}}, \lambda_{\mathrm{b}}} L(\theta, \lambda_{\mathrm{r}}, \lambda_{\mathrm{b}}). \tag{4}
$$

Besides SA-PINN, we consider layer-wise adaptive activation functions to further ameliorate the approximation capabilities of our PINN model [28]. In particular, we use for all $i = 1, \ldots, M$, $\sigma_i : x \mapsto \tanh(\alpha_i x)$, where $(\alpha_i)_i$ are trainable coefficients to be minimized along with the network weights and biases. In a slight abuse of notation, we include $(\alpha_i)_i$ in the set of trainable parameters θ.

4. Numerical Studies

In this section, we compare the approximation capability of the previously discussed PINN model when applied to Problems 2.1 and 2.2. For the sake of comparability, we use the same network architecture and hyper parametrization for both cases. In particular, the employed ANN consists of $M = 10$ hidden layers with $N_i = 45$ neurons, for all $i = 1, \ldots, M$.
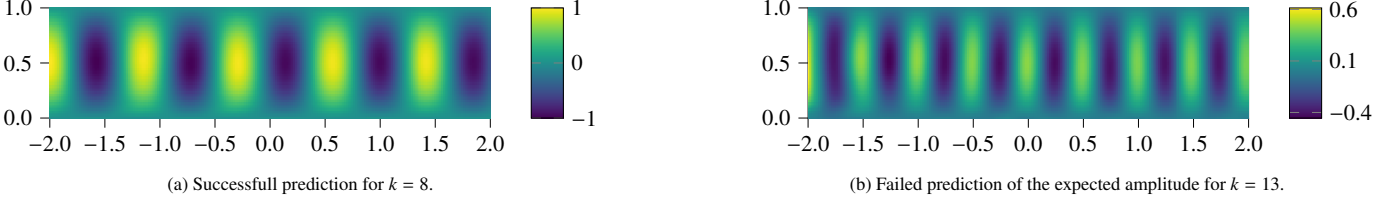
(a) Successfull prediction for $k = 8$.

(b) Failed prediction of the expected amplitude for $k = 13$.

Figure 2: Visualization of the real part of the PINN's prediction $\hat{u} := u_\theta$ using Problem 2.1 after 50000 Adam training steps.
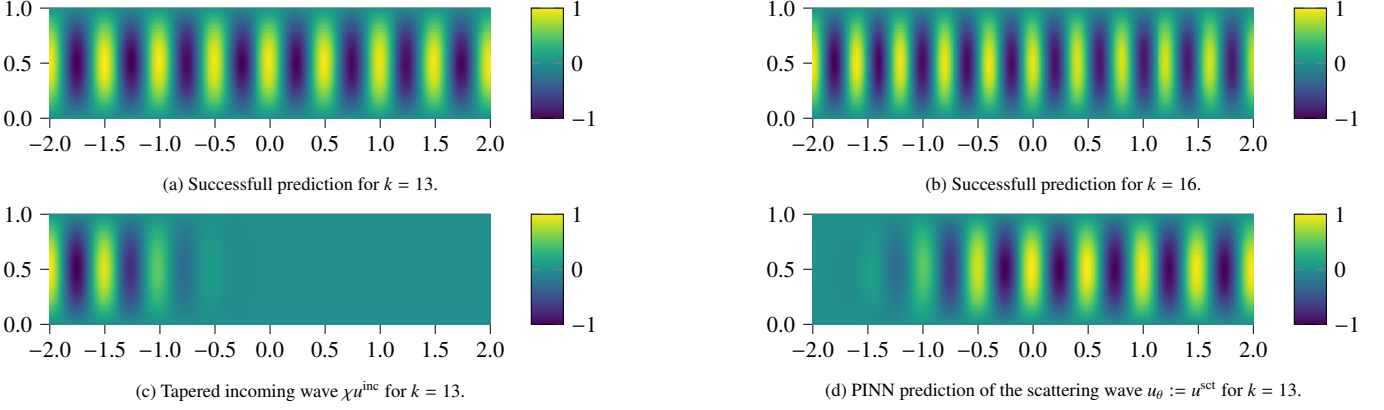

(a) Successfull prediction for $k = 13$.

(b) Successfull prediction for $k = 16$.

(c) Tapered incoming wave χu^{inc} for $k = 13$.

(d) PINN prediction of the scattering wave $u_\theta := u^{\mathrm{sct}}$ for $k = 13$.

Figure 3: Visualization of the real part of the reconstructed solution $\hat{u} := u_\theta + \chi u^{\mathrm{inc}}$ and its constituents using Problem 2.2 after 50000 Adam training steps.

As mentioned in the previous section, we consider adaptive hyperbolic tangents as activation functions initialized with $\alpha_i = 2$, for $i = 1, \ldots, M$, whereas the remaining trainable parameters of θ are initialized using a Glorot normal initializer.

For the sake of simplicity, we consider a rectangular waveguide junction $\Omega := (-b, b) \times (0, 1)$, $b = 2$. With the boundaries of Ω, $\Gamma_{0,1}$, $\Gamma_{0,2}$, Γ_-, and Γ_+ corresponding to Γ_j, $j = 1, \ldots, 4$ in (2), respectively, and by assigning accordingly the right-hand sides, we arrive at a loss function for Problems 2.1 and 2.2 similar to (3). Thereby, the interior and boundary points x_{r} and x_{b_j} are taken as a uniform grid of size $(120, 10)$, and with $N_{\mathrm{b}_j} := N_{\mathrm{b}} = 80$ for all $j = 1, \ldots, 4$, respectively. Moreover, we define the considered self-adaptive mask function by $m : x \mapsto x^2$, and draw the initial self-adaptive weights from uniform distributions as $\lambda_{\mathrm{r}} \sim (\mathcal{U}(0, 0.5))^{N_{\mathrm{r}}}$, $\lambda_{b_j} \sim (\mathcal{U}(0, 30))^{N_{\mathrm{b}}}$, for $j = 1, 2$, and $\lambda_{b_j} \sim (\mathcal{U}(0, 10))^{N_{\mathrm{b}}}$, for $j = 3, 4$. To solve (4), we employ an Adam optimizer with an exponential learning rate decay (with a rate of 0.95 every 1000 steps). With this, a training process consists of 50000 steps. All computations are performed using a TensorFlow v2.11.0 implementation in Python v3.10.12. To ensure reproducibility of the results, we choose the number 11 as seed for the generation of pseudo-random numbers.

In the following experiments, we assume that only the first mode propagates through the waveguide, i.e., in Definition 2.1, we assume $n = 1$. Moreover, the incoming wave reads

$$u^{\mathrm{inc}}(x, z) = \frac{1}{\sqrt{2}} e^{i(x+b) \cdot \lambda_1} \phi_1(z), \quad (x, z) \in \Omega.$$

Note that in the considered case of a simple rectangular wave-guide junction, the energy transmission is total, hence the expected exact solution u_{ref} corresponds to the incoming wave propagating along the x-axis.

On one hand, we notice that the prediction results of our PINN model using the ansatz $\hat{u} := u_\theta = u$ in Problem 2.1, i.e, when applied to the classical Helmholtz BVP are only successful up to $k = 8$. In Figure 2a, we illustrate the real part of the predicted solution for a successful example at $k = 8$. By increasing the wave number, we observe that the PINN solution starts to degenerate. In particular, the predicted amplitude decreases with higher k. For example, we showcase this effect for $k = 13$ in Figure 2b. On the other hand, the application of the same model on the equivalent formulation with $u_\theta = u^{\mathrm{sct}}$ in Problem 2.2 seems to clearly ameliorate the approximation capacity in dependence of k. This is visualized in Figure 3. In particular, Figure 3a shows the reconstructed solution $\hat{u} := u_\theta + \chi u^{\mathrm{inc}}$ for $k = 13$, which is in agreement with the expected solution. Moreover, we verify that this improvement is maintained up to $k = 16$, see, e.g., Figure 3b. For convenience, the constituents of $\hat{u}$, namely, the PINN prediction u_θ and χu^{inc} are plotted in Figure 3c and Figure 3d, respectively. Furthermore, we compare in Table 1 the prediction results for different wave numbers k using both formulations. For this, we use as metric the relative error with $\| \cdot \|_2$ being the Euclidean norm

$$\varepsilon(u) := \frac{\|u - u_{\mathrm{ref}}\|_2}{\|u_{\mathrm{ref}}\|_2}, \qquad (5)$$

and denote the PINN-based solution again by $\hat{u}$. Note that the latter is understood as $\hat{u} := u_\theta$ for Problem 2.1 and as $\hat{u} = u_\theta + \chi u^{\mathrm{inc}}$ for Problem 2.2.

4

	k	8	9	10	13	15	16
Prob. 2.1	ε_{R}	0.057	0.158	0.21	0.58	–	–
	ε_{I}	0.059	0.15	0.22	0.6	–	–
Prob. 2.2	ε_{R}	0.018	0.024	0.028	0.036	0.071	0.09
	ε_{I}	0.012	0.023	0.038	0.045	0.089	0.1

Table 1: Relative errors $\varepsilon_{\mathrm{R}} := \varepsilon(\Re\{\hat{u}\})$ and $\varepsilon_{\mathrm{I}} := \varepsilon(\Im\{\hat{u}\})$ w.r.t. the real and imaginary parts of $\hat{u}$, respectively (denoted by $\Re\{\hat{u}\}$ and $\Im\{\hat{u}\}$) for Problems 2.1 and 2.2 at different k.

The accuracy of the trained models is computed for $k = 8, 9, 10, 13, 15, 16$. We notice the expected amelioration even for $k = 8$, where the classical formulation in Problem 2.1 is sufficient to successfully learn the solution in the waveguide junction. However, it should also be noted that the formulation of Problem 2.2 does not completely circumvent the spectral bias but reduces it. This can be seen from the increasing error in both cases with increasing wave numbers k. Besides extending the range of possible wave numbers, the considered equivalent formulation accelerates the training procedures, as the same accuracy is reached at a significantly earlier stage of the training. For instance, Figure 4 shows the evolution of the training error for the solution's real part $\Re\{\hat{u}\}$ w.r.t. the training iterations at $k = 8$, where both an improved and more accurate learning can be distinguished.
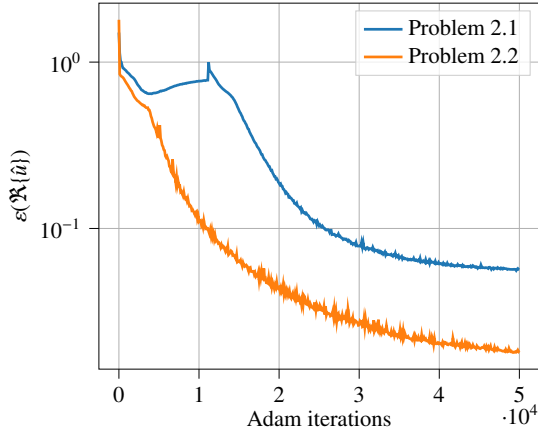

Figure 4: Comparison of the learning dynamics using the relative error (5) w.r.t. the real part of the predicted solution $\hat{u}$ (denoted by $\Re\{\hat{u}\}$) from Problems 2.1 and 2.2 with $k = 8$. The relative error is evaluated for visualization purpose once each 100 iterations.

5. Summary and Conclusion

We proposed an equivalent taper-based scattering formulation of the two-dimensional Helmholtz BVP by introducing inhomogeneities to the BVP through a splitting of the solution. We numerically illustrated that the resulting equivalent formulation improves and accelerates the learning process of our PINN model, as it reduces the tendency of our model when applied to the classical formulation of the Helmholtz BVP, to learn the zero function. This allowed for more accurate solutions and extended the range of successfully predictable wave numbers. Although our numerical experiments were limited to straight waveguide junctions, it is possible to consider more complex geometrical configurations. Moreover, it should be noted that other shapes for the taper-function are conceivable, including non-polynomial functions. In addition, the taper-based scattering formulation is not restricted to the first mode, allowing for future extensions to consider higher modes for the incoming wave and the DtN operator.

Declaration of competing interest

The authors declare that they have no known competing financial interests or personal relationships that could have appeared to influence the work in this paper.

List of abbreviations

Adam	Adaptive moment estimation
ANN	Artificial Neural Network
BVP	Boundary Value Problem
DtN	Dirichlet-to-Neumann
FEM	Finite Element Method
PINN	Physics-Informed Neural Network
SA-PINN	Self-Adaptive Physics-Informed Neural Network
XPINN	Extended Physics-Informed Neural Network
NTK	Neural Tangent Kernel

References

[1] M. Raissi, P. Perdikaris, G. E. Karniadakis, Physics-informed neural networks: A deep learning framework for solving forward and inverse problems involving nonlinear partial differential equations, Journal of Computational Physics 378 (2019) 686–707. doi:10.1016/j.jcp.2018.10.045.

[2] M. Raissi, A. Yazdani, G. E. Karniadakis, Hidden fluid mechanics: Learning velocity and pressure fields from flow visualizations, Science 367 (6481) (2020) 1026–1030. doi:10.1126/science.aaw4741.

[3] F. Sahli Costabal, Y. Yang, P. Perdikaris, D. E. Hurtado, E. Kuhl, Physics-Informed Neural Networks for Cardiac Activation Mapping, Frontiers in Physics 8 (2020) 42. doi:10.3389/fphy.2020.00042.

[4] Z. Mao, A. D. Jagtap, G. E. Karniadakis, Physics-informed neural networks for high-speed flows, Computer Methods in Applied Mechanics and Engineering 360 (2020) 112789. doi:10.1016/j.cma.2019.112789.

[5] A. D. Jagtap, Z. Mao, N. Adams, G. E. Karniadakis, Physics-informed neural networks for inverse problems in supersonic flows, Journal of Computational Physics 466 (2022) 111402. `doi:10.1016/j.jcp.2022.111402`.

[6] Y. Chen, L. Lu, G. E. Karniadakis, L. Dal Negro, Physics-informed neural networks for inverse problems in nano-optics and metamaterials, Optics express 28 (8) (2020) 11618–11633. `doi:10.1364/oe.384875`.

[7] I. Depina, S. Jain, S. Mar Valsson, H. Gotovac, Application of physics-informed neural networks to inverse problems in unsaturated groundwater flow, Georisk: Assessment and Management of Risk for Engineered Systems and Geohazards 16 (1) (2022) 21–36. `doi:10.1080/17499518.2021.1971251`.

[8] S. Cuomo, V. S. Di Cola, F. Giampaolo, G. Rozza, M. Raissi, F. Piccialli, Scientific Machine Learning Through Physics-Informed Neural Networks: Where we are and What's Next, Journal of Scientific Computing 92 (3) (2022) 88. `doi:10.1007/s10915-022-01939-z`.

[9] N. Rahaman, A. Baratin, D. Arpit, F. Draxler, M. Lin, F. Hamprecht, Y. Bengio, A. Courville, On the Spectral Bias of Neural Networks, in: K. Chaudhuri, R. Salakhutdinov (Eds.), Proceedings of the 36th International Conference on Machine Learning, Vol. 97 of Proceedings of Machine Learning Research, PMLR, 2019, pp. 5301–5310.
URL `https://proceedings.mlr.press/v97/rahaman19a.html`

[10] S. Wang, X. Yu, P. Perdikaris, When and why PINNs fail to train: A neural tangent kernel perspective, Journal of Computational Physics 449 (2022) 110768. `doi:https://doi.org/10.1016/j.jcp.2021.110768`.

[11] S. Wang, H. Wang, P. Perdikaris, On the eigenvector bias of fourier feature networks: From regression to solving multi-scale pdes with physics-informed neural networks, Computer Methods in Applied Mechanics and Engineering 384 (2021) 113938. `doi:https://doi.org/10.1016/j.cma.2021.113938`.

[12] L. D. McClenny, U. M. Braga-Neto, Self-adaptive physics-informed neural networks, Journal of Computational Physics 474 (2023) 111722. `doi:10.1016/j.jcp.2022.111722`.

[13] A. D. Jagtap, G. E. Karniadakis, Extended physics-informed neural networks (XPINNs): a generalized space-time domain decomposition based deep learning framework for nonlinear partial differential equations, Communications in Computational Physics 28 (5) (2020) 2002–2041. `doi:10.4208/cicp.oa-2020-0164`.

[14] L. Bourgeois, E. Lunéville, The linear sampling method in a waveguide: a modal formulation, Inverse Problems 24 (1) (2008) 015018. `doi:10.1088/0266-5611/24/1/015018`.

[15] T. Arens, D. Gintides, A. Lechleiter, Variational formulations for scattering in a three-dimensional acoustic waveguide, Mathematical Methods in the Applied Sciences 31 (7) (2008) 821–847. `doi:10.1002/mma.947`.

[16] J. Ott, Domain Optimization for an Acoustic Waveguide Scattering Problem, Applied Mathematics and Optimization 72 (1) (2015) 101–146. `doi:10.1007/s00245-014-9273-1`.

[17] O. G. Ernst, M. J. Gander, Why it is Difficult to Solve Helmholtz Problems with Classical Iterative Methods, in: Numerical Analysis of Multiscale Problems, Springer Berlin Heidelberg, 2011, Ch. 10, p. 325–363. `doi:10.1007/978-3-642-22061-6_10`.

[18] G. C. Diwan, A. Moiola, E. A. Spence, Can coercive formulations lead to fast and accurate solution of the Helmholtz equation?, Journal of Computational and Applied Mathematics 352 (2019) 110–131. `doi:https://doi.org/10.1016/j.cam.2018.11.035`.

[19] C. Song, T. Alkhalifah, U. B. Waheed, A versatile framework to solve the Helmholtz equation using physics-informed neural networks, Geophysical Journal International 228 (3) (2022) 1750–1762. `doi:10.1093/gji/ggab434`.

[20] P. Escapil-Inchauspé, G. A. Ruz, Hyper-parameter tuning of physics-informed neural networks: Application to Helmholtz problems, Neurocomputing 561 (2023) 126826. `doi:https://doi.org/10.1016/j.neucom.2023.126826`.

[21] C. Song, Y. Wang, Simulating seismic multifrequency wavefields with the Fourier feature physics-informed neural network, Geophysical Journal International 232 (3) (2023) 1503–1514. `doi:10.1093/gji/ggac399`.

[22] S. Schoder, F. Kraxberger, Feasibility study on solving the Helmholtz equation in 3D with PINNs (2024). `doi:10.48550/ARXIV.2403.06623`.

[23] A. G. Baydin, B. A. Pearlmutter, A. A. Radul, J. M. Siskind, Automatic Differentiation in Machine Learning: a Survey, Journal of Machine Learning Research 18 (1) (2017) 5595–5637.

[24] D. P. Kingma, J. Ba, Adam: A Method for Stochastic Optimization (2014). `doi:10.48550/ARXIV.1412.6980`.

[25] X. Glorot, Y. Bengio, Understanding the difficulty of training deep feedforward neural networks, in: Y. W. Teh, M. Titterington (Eds.), Proceedings of the Thirteenth International Conference on Artificial Intelligence and Statistics, Vol. 9 of Proceedings of Machine Learning Research, PMLR, Chia Laguna Resort, Sardinia, Italy, 2010, pp. 249–256.
URL `https://proceedings.mlr.press/v9/glorot10a.html`

[26] K. He, X. Zhang, S. Ren, J. Sun, Delving Deep into Rectifiers: Surpassing Human-Level Performance on ImageNet Classification, in: 2015 IEEE International Conference on Computer Vision (ICCV), 2015, pp. 1026–1034. `doi:10.1109/ICCV.2015.123`.

[27] A. A. Heydari, C. A. Thompson, A. Mehmood, Softadapt: Techniques for adaptive loss weighting of neural networks with multi-part loss functions (2019). `doi:10.48550/ARXIV.1912.12355`.

[28] A. D. Jagtap, K. Kawaguchi, G. E. Karniadakis, Adaptive activation functions accelerate convergence in deep and physics-informed neural networks, Journal of Computational Physics 404 (2020) 109136. `doi:https://doi.org/10.1016/j.jcp.2019.109136`.